Highly efficient CuO/ZnO/ZrO$_2$@SBA-15 nanocatalysts for methanol synthesis from the catalytic hydrogenation of CO$_2$

Mauro Mureddu[*], Francesca Ferrara, Alberto Pettinau

Sotacarbo S.p.A., Grande Miniera di Serbariu, 09013, Carbonia, Italy

ARTICLE INFO

Keywords:
CO$_2$ hydrogenation
Methanol synthesis
CuO/ZnO/ZrO$_2$ catalysts
SBA-15
Nanocomposite

ABSTRACT

Cu/ZnO@SBA-15 and Cu/ZnO/ZrO$_2$@SBA-15 nanocomposites have been synthesized by an innovative impregnation-sol-gel autocombustion combined strategy and tested as catalysts for carbon dioxide hydrogenation to methanol. The composites, differing as to the active phase loading (20 and 35 wt.%) and Cu/Zn molar ratio (1.0-2.5 mol mol^{-1}), have been characterized in terms of chemical, morphological, structural and textural features by a multi-technique approach. Characterization techniques revealed that the active phase is highly dispersed into/over the well-ordered mesoporous channels especially at low loading and low Cu/Zn molar ratio. In all the composites, the mesostructure of the support is retained together with a high surface area, large pore volume and uniform pore size. Catalytic results showed that the supported catalyst with the lowest Cu/Zn molar ratio (1.0 mol mol^{-1}) exhibits the best catalytic performance with a space-time-yield of methanol of 376 mg$_{CH3OH}$ h^{-1} g$_{cat}$$^{-1}$, much more efficient than the unsupported catalyst (10 mg$_{CH3OH}$ h^{-1} g$_{cat}$$^{-1}$). The confinement of the active phase in the SBA-15 structure enhances its ability to interact with H$_2$ and CO$_2$, which results in improved performance. Moreover, the results show the influence of the active phase loading and the Cu/Zn molar ratio that lead to differences in the morphology and dispersion of the active phase, which in turn cause the composite to catalyse the reaction differently.

1. Introduction

Increasing attention toward climate changes and the recent strategic policies to stabilize and reduce the amount of CO$_2$ emissions have resulted in the promotion of research in the field of carbon capture and storage, whereby CO$_2$ is captured from industrial flue gases and permanently stored in geological formations, such as depleted oil or gas fields and saline aquifers [1]. In parallel, the greater diffusion of power generation plants from renewable sources (in particular wind and solar) is making the development of technologies for energy storage a priority in order to stabilize the electrical grid [2], balancing production and demand, and thus avoiding the inefficient use of fossil fuel power plants.

In this scenario, CO$_2$ utilization technologies are expected to play a very important role in both these areas [3,4]. In fact, captured CO$_2$ can be considered not just as a residue to be permanently stored, but – combined with hydrogen from renewable sources – as a resource for the production of energy carriers, such as methanol, dimethyl ether and many other liquid or gaseous fuels [5]. From this perspective, CO$_2$ utilization could contribute to the containment of global warming, since the CO$_2$ products can replace the corresponding products from

fossil fuels [6]. In parallel, CO$_2$-to-liquids can be seen as a sort of chemical energy storage, as the hydrogen is produced by water electrolysis using the overproduction of electricity from renewable sources [7]. One way to accomplish this is by exploring highly active and selective catalysts for methanol synthesis, because of the thermodynamic stability of CO$_2$ [8]. While many catalytic systems including supported precious metal catalysts have been investigated, Cu/ZnO-based catalysts remain the most promising system for methanol synthesis from CO$_2$ [9,10].

As an alternative to Cu-Zn-Al catalysts, conventionally used for methanol synthesis from syngas [11–18], many authors have found that Cu-Zn-Zr catalysts are particularly effective for methanol synthesis from CO$_2$ hydrogenation [19–25]. Although methanol via CO hydrogenation has been industrialized, catalysts for CO$_2$ hydrogenation to methanol still have to deal with the obstacles resulting from poor stability, particularly for supported metal catalysts under industrial conditions [26]. In the real environment, the activity loss of these catalysts is attributed to thermal degradation via sintering of Cu particles [27–29]. ZnO is an important component because it prevents the agglomeration of Cu particles, thus leading to the large Cu surface area needed for methanol synthesis. Water produced during methanol synthesis from a CO$_2$-rich

feed accelerates the crystallization of Cu and ZnO leading to the deactivation of the catalyst [30]. A possible way to overcome such drawbacks could be the dispersion of the active phase onto a suitable, high-surface area support [31]. The addition of supports improves the catalytic and mechanical properties by increasing the surface area, stabilizing the particles from sintering [32], keeping the catalyst away from structure breakage during the reaction and stabilizing the active phase [33]. Microporous supports are inappropriate due to the severe mass transfer limitations associated with their microporous system. Furthermore, although showing high surface area, they do not allow dispersing the active phases in form of nanoparticle inside the pores, so particles with broad size distribution are commonly obtained over the surface and sintering phenomena are observed. The discovery of ordered mesoporous molecular sieves (known as the M41S family) has expanded the range of uniform pore size from the micropore to the mesopore regime. Among them, MCM-41 having thin wall thickness is not thermally stable. Particularly interesting is the mesostructured SBA-15 silica, a high-surface area (up to 1000 m^2/g) material, with 6–7 nmwide regular channels and thick (3–4 nm) pore walls [34]. With the confinement of the active metal-oxide phase into the mesoporous channels of SBA-15, the nanostructured oxide would be sinter-resistant as well as showing superior metal dispersion, and a consequent enhancement of the active phase reactivity might be expected [35–39]. SBA-15 represents an ideal support owing to several reasons; (*i*) the ordered mesoporous structure allows the formation of active nanophases with narrow particle size distribution, (*ii*) the size of pores allow the easy diffusion of the gaseous molecules and the easy accessibility to the active phase inside the pores, (*iii*) the wall thickness ensures the thermal stability of the support, especially in view of the high pressure and temperature required by the reaction, and hamper sintering phenomena during the use of the catalyst.

As a result, the copper/zinc oxide/zirconia@SBA-15 composite would behave as an ideal reactor, with the mesopores acting as channels for the rapid transport of the reactant. To the best of the present authors' knowledge, very few papers dealing with the use of SBA-15 as a support for copper, or copper and zinc oxide have been published so far. The performance of Cu/ZnO phase supported on SBA-15 in the methanol synthesis from syngas, and not from pure CO_2, have been evaluated [40], and only one study investigated such a system for the catalytic hydrogenation of CO_2 to methanol [41,42]. In all the above mentioned cases, a long reaction time study is not considered.

An overwhelming majority of studies in the field of methanol synthesis are dedicated to optimizing processes that require relatively high pressure (50–100 bar). This pressure range is relevant for industrial applications, but such processes involve large scale production units, high operational and investment costs. The efficiency of methanol synthesis is limited by thermodynamics owing to the severe exothermic reaction. The low-temperature process is also beneficial from thermodynamic point of view: methanol production is an exothermal reaction; this implies that low temperatures should in principle promote formation of the alcohol. On the other hand, high pressure shifts the equilibrium to the right due to entropy considerations. As a result, developing a low-temperature and low-pressure process will greatly reduce the production cost and high single-pass CO_2 conversion will become available at low temperature. A key factor in converting carbon dioxide to methanol is finding a good catalyst so that methanol can be produced in high selectivity at an efficient rate.

Particle size, surface area, metallic Cu^0 surface area and composition of the catalyst are important factors that affect catalytic activity and methanol selectivity. These factors are influenced by different catalyst synthesis methods. Different methods have been proposed with the aim to optimize the final catalytic performance. Preparation methods of metal oxide supported nanoparticles usually involve the deposition of a metal precursor from the liquid phase on preformed support by different impregnation or deposition-precipitation procedure. Nonetheless, conventional methods can result in the deposition of

a large amount of precursor material at the exterior parts of the support bodies during drying and the resulting heterogeneous materials display an "egg-shell" distribution of the active component, or can lead to inhomogeneous distributions after drying [43–45]. To prevent redistribution of the precursor during drying, special measures have to be taken, *e.g.*, by carefully controlling the drying rate of the impregnated bodies [46]. Another option to overcome the redistribution of precursor compound during drying involves the use of chelated precursor complexes. Some authors have stated that the prevention of redistribution during drying is the key to obtaining a highly dispersed and homogeneously distributed metal (oxide) phase [43]. Several studies claim that the use of chelating salts, or the addition of viscosityincreasing agents to aqueous nitrate solutions, prevents the formation of "eggshell" type distributions [43,47–49]. In addition to the homogeneous precursor distributions, the metal dispersion of the final catalyst has also been found to increase significantly with these chelating precursor salts.

For the first time, this study brings together the positive effects of the sol-gel autocombustion chemical procedure and the advantage derived from the confinement of the active phase into/over the SBA-15 mesochannels; it is resulted in a specific catalyst for the catalytic hydrogenation of the CO_2 to methanol. This strategy has been designed in order to trigger the autocombustion inside the mesochannels of the SBA-15 with the aim of obtaining an active phase with different and improved features compared to those derived from a conventional impregnation or a simply autocombustion. With the confinement of the active metal-oxide phase into the mesoporous channels of SBA-15, an improved metal-oxide dispersion has been obtained, and a consequent enhancement of the active phase reactivity might be expected together with an enhanced interaction between the reactants (H_2 and CO_2).

Moving along this line, this study focuses on an innovative nanocatalysts preparation of both copper/zinc oxide@SBA-15, and copper/zinc oxide/ zirconium oxide@SBA-15 systems via a novel combined strategy of impregnation-sol-gel autocombustion whose behaviour in methanol synthesis from carbon dioxide hydrogenation was investigated at 250 °C and 3.0 MPa with the aim of correlating the catalyst's performance with its physico-chemical features. The behaviour of the catalysts supported on SBA-15 in the methanol synthesis from an H_2/CO_2 stream has been investigated in a fixed-bed stainless-steel reactor and compared with that of an unsupported copper/zinc oxide/zirconium oxide catalyst.

Concerning the novel "*in situ* autocombustion method of a glycinenitrate complex in mesoporous silica", very few studies have dealt with the use of SBA-15 as a support for different active phases including CuO [50], LaCoO$_3$ [51], and Fe$_2$O$_3$ [52]. However, most of the work that has been done has focused on different reactions, such as the catalytic wet peroxide oxidation or methane oxidation.

The morphological, structural, and textural features of fresh and used catalysts have been assessed by a multi-technique approach. The structural features of all the catalysts have been evaluated by X-ray diffraction (XRD) and transmission electron microscopy (TEM), and their textural properties have been investigated by N_2 physisorption. The active phase is in the form of a thin amorphous layer or small nanoparticles that have been highly dispersed into/over well-ordered mesoporous silica channels. The efficient incorporation of the active phase into SBA-15 resulted in a considerable improvement of the catalytic performance compared to the unsupported one and the most recent data reported in the literature. The influence of an extended time on stream (T.o.S.) has also been investigated. Thanks to the encouraging results outlined here, the obtained catalyst is the subject of the PCT (Patent Cooperation Treaty) application number PCT/EP2019/053068: "Efficient catalyst for the conversion of CO_2 to methanol".

2. Experimental

2.1. Materials

Mesostructured SBA-15 silica (SiO_2, 99%) with a long-range-order structure was purchased from Sigma-Aldrich. All of the chemicals required (analytical-grade), used as received without any further purification, have been purchased from Sigma-Aldrich. The supported Cu/ZnO@SBA-15 (CZS series) and Cu/ZnO/ZrO_2@SBA-15 (CZZS series) catalysts have been synthesized through a novel impregnation-sol-gel autocombustion combined strategy. For comparative purpose, an unsupported Cu/ZnO/ZrO_2 (CZZ series) catalyst with the same composition was prepared using the same glycine-nitrate combustion method.

2.2. Preparation of catalysts

2.2.1. Supported catalysts

Two series of copper/zinc oxide and copper/zinc oxide/zirconium oxide both supported on SBA-15 have been prepared with different active phase loading (20 and 35 wt.%) and different Cu/Zn molar ratio (1.0 and 2.5 mol mol^{-1}). First, an aqueous solution of the metal nitrates is prepared and then an aqueous solution of glycine is added to the first to obtain the "impregnation solution". Typically, the procedure for the CZZS series with an active phase of 20 wt.% is the following: 32 cm^3 of aqueous solution containing $Cu(NO_3)_3 \cdot 3H_2O$ (Aldrich, 99%, 4.3 mmol), $Zn(NO_3)_2 \cdot 6H_2O$ (Aldrich, 98%, 1.7 mmol), $Zr(NO_3)_4 \cdot 5H_2O$ (Aldrich, 99%, 2.6 mmol) and glycine (Aldrich, ≥98%, 12.4 mmol) is put into contact dropwise with 3.2 g of freshly calcined silica under vigorous stirring (about 700 rpm) at room temperature. The sky blue dispersion has a spontaneous pH value 2.50 ± 0.01 and water is slowly allowed to evaporate into the air. The viscous sky blue gel collected after evaporation is treated for 5 min in an ultrasonic bath, and then submitted to a sudden rise of temperature up to 300 °C for 1 h, activating the combustion mechanism and decomposing the metal nitrates, generating an olive green dry powder. The solids are then characterized and catalytically tested without further thermal treatment. The obtained supported catalysts are labelled as CZS_X_Y and CZZS_X_Y, where X indicates the active phase loading and Y denotes the Cu/Zn molar ratio.

2.2.2. Unsupported Cu/ZnO/ZrO₂ catalyst as a reference for methanol synthesis

$Cu(NO_3)_3 \cdot 3H_2O$ (Aldrich, 99%, 10 mmol), $Zn(NO_3)_2 \cdot 6H_2O$ (Aldrich, 98%, 4.2 mmol) and $Zr(NO_3)_4 \cdot 5H_2O$ (Aldrich, 99%, 6.25 mmol), used as sources of metal ions, are dissolved in deionized water to form a clear blue solution matching the formula $(CuO)_{0.5}(ZnO)_{0.2}(ZrO_2)_{0.3}$. Then, an aqueous solution of glycine (Aldrich, ≥98%, 30 mmol) used as chelating-fuel agent is prepared and mixed together with the aqueous solution of metal salts into a Pyrex beaker. The molar ratio of metals (Cu (II) + Zn(II) + Zr(IV)) to glycine is fixed at 1:1.44. The corresponding equivalence ratio (ϕ_e = oxidizer/fuel ratio) is equal to 0.69. The clear pale blue solution thus obtained has a spontaneous pH 1.50 ± 0.01 and is allowed to evaporate on a hot plate maintaining the solution temperature at 100-120 °C. As a result of the increasing concentration, the viscosity rises due to the crosslinking of glycinemetal complexes into a three dimensional structure [53], with ionic metal-glycine, or hydrogen bonds, and, on further dehydration, a gel starts to form. Later, the gel is put in a preheated oven and submitted to a sudden rise of temperature up to 500 °C, that brings about the boiling and the swelling of the gel with the evolution of a large quantity of nontoxic gases (CO_2, H_2O, N_2) [54]. The autocombustion is complete within few seconds giving rise to dark brown, with metallic reflections, branched voluminous powders. The obtained unsupported catalyst is labelled as CZZ.

2.3. Characterization of materials

Inductively coupled plasma atomic emission spectroscopy (ICP-AES)

analyses have been performed with a Liberty 200 spectrophotometer (Varian) to determine the final metal oxide content and the chemical composition in terms of Cu/Zn molar ratio. Samples (*ca.* 0.015 g) are first dissolved in concentrated hydrofluoric acid (40%); after evaporation, the residues are dissolved in a mixture of HCl (37%) and HNO_3 (70%) (3:1 by volume) and then diluted to 250 cm^3 with Milli-Q water.

Low-angle ($2\theta = 0.8$–$2.5°$) and wide-angle ($2\theta = 10$-$70°$) X-ray diffraction patterns are recorded on a Seifert X3000 diffractometer with a θ-θ Bragg Brentano geometry with Cu Kα wavelength. Low-angle diffraction patterns are recorded using a zerobackground silicon sample holder. The coherent domain (crystallite size) is obtained by Scherrer's equation using the Warren correction [55].

Transmission Electron Microscopy (TEM) investigation has been carried out using a Jeol 200CX microscope operating at an accelerating voltage of 200 kV. Finely ground samples are dispersed in *n*-octane and subjected to an ultrasonic bath and the suspensions are then dropped on carbon-coated copper grids for the TEM observations.

Textural analysis has been carried out on a Sorptomatic 1990 System (Fisons Instrument) by determining the nitrogen adsorption/desorption isotherms at −196 °C. Prior to analysis, the samples are heated overnight under vacuum up to 220 °C (heating rate 1 °C/min). The Brunauer-Emmett-Teller (BET) specific surface area and pore volume are assessed from the adsorption data. The mean pore diameter is determined by applying the Barrett-Joyner-Halenda (BJH) model to the isotherm desorption branch [56].

TPR profiles have been recorded on a TPD/R/O 1100 apparatus (Thermo Fisher Scientific), under the following conditions: sample weight of 0.030 g; heating rate from 40 to 400 °C of 10 °C min^{-1}; flow rate of 30 cm^3 min^{-1}; H_2 concentration of 5% v/v in N_2. Prior to the experiment, samples are pre-treated in nitrogen (20 cm^3 min^{-1}) at 350 °C for 2 h. The hydrogen consumption is monitored by a thermal conductivity detector (TCD).

The copper surface area (S_{Cu}) has been evaluated by dissociative N_2O adsorption and carried out in a U-tube quartz reactor (the same used for the determination of the TPR profiles) with a thermal conductivity detector (TCD) to monitor the consumption of H_2 and expressed both as m_{Cu}^0/g_{ctz} (A_{sam}) and m_{Cu}^0/g_{Cu} (A_{met}). N_2O reacts with metallic Cu on the catalyst surface to form Cu_2O and N_2 [57]. The procedure used is the following: 0.30 g of fresh catalyst is first reduced in 5% v/v H_2/N_2 mixture for 1 h at 250 °C with a heating rate of 10 °C min^{-1}; reactive N_2O/He gas mixture gas at 40 °C is passed to ensure complete oxidation of metallic copper to Cu^+; catalyst is reduced again with a temperature programmed reduction in 5 vol.% H_2/N_2 from 40 °C to 400 °C, with a heating rate of 10 °C min^{-1}.

The copper surface area is calculated from the amount of N_2O reacted considering a reaction stoichiometry of N_2O:Cu of 1:2 and an atomic copper surface density of 1.46×10^{19} Cu atoms/m^2. The area under the peak of H_2, caused by associative desorption of H_2 from copper metal surface, is used to determine the copper surface area from the following equation:

Cu surface area (m^2 g^{-1}) = (A) x (S) x (NA) / SD_{Cu}

where *A* is the amount of H_2 desorbed from the TPR peak (mol H_2 g_{cat}^{-1}), *S* the stoichiometric factor (2), *NA* is the Avogadro's number (6.022×10^{23} atoms mol^{-1}), SD_{Cu} is the copper surface density (1.46×10^{19} Cu atoms/m^2).

Copper dispersion, defined as the amount of H_2 desorbed from the TPR peak divided by the total copper atoms present in the catalyst, is calculated by the following equation:

Cu dispersion (%) = (A) x (S) x (MW_{Cu}) / Cu content (wt.%) *100

2.4. Catalyst testing

The methanol synthesis experiments have been carried out in a commercial customized Microactivity Efficient, PID Eng&Tech bench-scale plant, employing a high-pressure fixed bed stainless steel reactor (9.1 mm I.D. x 304.8 mm long,). A porous plate (made of Hastelloy C, 20 μm in size) and quartz wool is used to support the catalytic bed (0.45 g) inside the isothermal temperature zone of the reactor. Typically, the reactor is loaded with 0.45 g of unsupported catalyst previously diluted with α-Al_2O_3, or 0.45 g of supported catalyst without dilution (SBA-15 is inert in the reaction), in order to obtain a total bed volume of *ca.* 3 cm^3. Prior to catalytic testing, all fresh catalysts are reduced *in-situ* in a stream of 10% v/v H_2/N_2 at 300 °C for 2 h under atmospheric pressure. Upon completion of the reduction process, the temperature is reduced to 250 °C, the reaction gas (CO_2:H_2:N_2 = 22.5:67.5:10, N_2 used as internal standard for gas-chromatographic analysis) is fed (with an inlet flow rate 333 cm^3 min^{-1}) and the system makes it possible to pressurize at 3.0 MPa. The steady-state activity measurements are taken after 1 h on the stream. The concentrations of the inlet gas and the reactor effluent are monitored by means of an online micro-gas chromatograph (SRA R3000) equipped with TCD detector for H_2, CO_2, CO and other possible hydrocarbons (CH_4, C_3H_8, C_4H_{10} etc.). Methanol and water in liquid effluent are analysed offline with a gas chromatograph coupled with a mass spectrometer (Agilent 7890A and Agilent 5977A MSD) equipped with a 25-m PoraPlot Q column (0.25 mm, narrowbore). The space time yield of methanol (STY$_{CH3OH}$), *i.e.* the amounts of methanol yield produced per gram of catalyst per hour (g_{CH3OH} g_{cat}^{-1} h^{-1}) is determined by the formula:

$$STY_{(CH3OH)} = (W_{Tot} * X(CH_3OH))/(t * m)$$

where W_{Tot} represents the total weight of methanol and water formed during the reaction (g), $X(CH_3OH)$ is the mass fraction of methanol, t indicates the time of reaction (h), m is the weight of the catalyst (g).

Methanol selectivity is calculated as follows:

$$S_{(CH3OH)} = (mole\ of\ CH_3OH\ produced)/(total\ mole\ of\ products)*100$$

All the catalytic studies have been performed three times for each catalyst and the values of the standard deviations obtained for the conversion and selectivity are in the range 2–5%.

3. Results and discussion

3.1. Fresh catalysts characterization

Table 1 shows the chemical composition of the fresh calcined CZS and CZZS catalyst series. The total active phase content and Cu/Zn molar ratio are in line with the nominal values.

The results of the structural characterization are summarized in Fig. 1. The low-angle diffraction patterns of the CZS and CZZS catalysts series are shown in Fig. 1a. Three well-resolved diffraction peaks, which can be indexed as the (100), (110) and (200) reflections associated with a hexagonal symmetry, are present in all the XRD patterns. This is in line with the presence of a two-dimensional hexagonal *P6mm* structure with a large unitcell parameter [34]. This indicates that the ordered
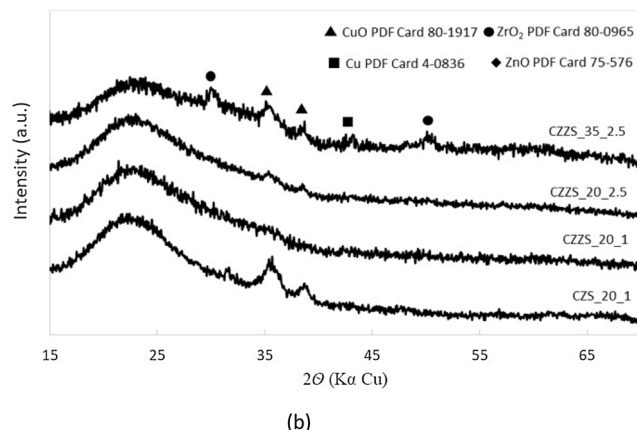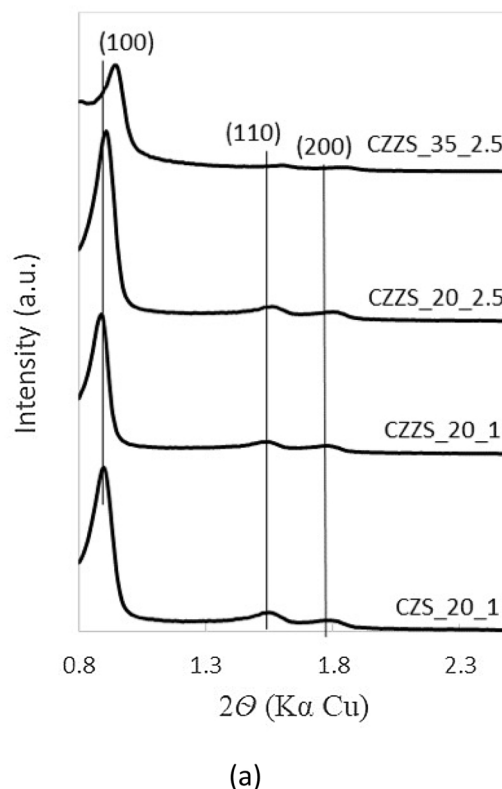

(a)

(b)

Fig. 1. XRD patterns of CZS and CZZS fresh catalysts at low-angle (a) and wide-angle (b). The main reflection planes are marked..

mesoporous structure of SBA-15 is retained after the auto-combustion process and incorporation of the active phase. A slight shift of the peaks towards higher values of 2θ seems to occur just for the CZZS_35_2.5 composite, suggesting a small contraction of the cell parameters.

The wide-angle diffraction patterns (Fig. 1b) show for all the samples the typical halo of amorphous silica at 2θ approximately 23°. No evident diffractions peaks corresponding to the copper-, zinc- or zirconium-oxide phases are observable in the CZZS_20_1 composite, and

Table 1
ICP-AES analysis of CZS and CZZS catalyst series.

Sample	Cu(ppm)	Zn(ppm)	Zr(ppm)	Cu/Zn(mol mol^{-1})	CuO(wt.%)	ZnO(wt.%)	ZrO$_2$(wt.%)	CuO + ZnO + ZrO$_2$(wt.%)
CZS_20_1	5.49	5.21	–	1.1	8.63	8.15	–	16.78
CZZS_20_1	6.60	6.20	7.51	1.1	6.31	5.89	7.74	19.94
CZZS_20_2.5	8.18	3.98	7.49	2.1	7.81	3.78	7.72	19.31
CZZS_35_2.5	5.74	2.88	5.52	2.3	14.61	7.28	15.16	37.05

only a very large band at 2θ = ca. 36° associable with the most intense reflections of ZnO or ZrO_2 phases occur. This indicates that the active phase is well dispersed into/over the support as an amorphous phase or as nanocrystals whose size is under the XRD detection limit. Besides the silica haloes, the pattern of the sample CZZS_20_2.5, and especially of the CZZS_35_2.5 sample with higher active phase content, exhibits clear wide peaks at 2θ = ca. 35.5° and 38.7° indicating the presence of monoclinic CuO (PDF Card 80–1917) and the relative intensity of the peaks is found to increase with the increase in active phase loading. Due to overlapping with the CuO reflections, the presence of ZnO cannot be ruled out. The mean particle size by applying the Scherrer equation – using the Warren correction – has been calculated for the CZS_20_1 and CZZS_35_2.5 composites through the determination of the FWHM of the reflections located at 35.5° and 38.7° associated with the copper oxide phase. In particular, a value close to 6 nm has been found for the CZZS_35_2.5 catalyst, and a value close to 5 nm has been calculated for the CZS_20_1 catalyst. Two additional peaks are clearly visible at 2θ = ca. 30° and 50.5° this can be attributed to the most intense reflections of the tetragonal ZrO_2 phase (PDF-CARD 80-0975). It is worth noting that in the CZZS_35_2.5 composite it is possible to observe the presence of a low intensity diffraction peak at 2θ = ca. 43.2° attributed to the most intense reflection (111) of the metallic Cu phase (PDF Card 4-0836). This finding could indicate that the "*in-situ* autocombustion procedure" makes it possible to obtain (at least partially) the copper directly in metallic state, but a mixture of copper oxide (Cu^{2+}) and metallic copper (Cu^0) is detected. All of the above results indicates that a good dispersion of the active phase over/into SBA-15 has been achieved.

Representative TEM images of the most significant supported catalysts are depicted in Figs. 2 and 3. As shown in Figs. 2 and 3 the wellordered 2D-hexagonal symmetry is observed in both the composites according to the low-angle XRD patterns where diffraction peaks characteristic of the hexagonal pore structure have been observed even after the autocombustion process and irrespective of the metal oxide content. TEM micrographs of the CZZS_20_1 sample (Figs. 2 a and 2b) do not show evident isolated metal oxide particles onto the external surface or inside the pore, but only a very slight shrinkage of the mesochannels is observable according to the BET results. This may suggest that the formation of an amorphous and quite uniform thin layer of metal oxide has occurred at the inner surface of the pore walls, in line with the XRD and BET data and as already observed by some authors [31,40]. Nevertheless, the pores remain completely open and the limited size of nanoparticles or thin layer do not result in any pore plugging. At variance with the case of CZZS_20_1, the most concentrated sample (CZZS_35_2.5) shows metal oxide nanoparticles with sizes (20–30 nm) larger than the pore size located on the surface (Fig. 3), outside the support. Figs. 3c and 3d are worthy of further comment; in some regions, the metal oxide particles with a rod-like morphology seem to fill up the SBA-15 channels with a diameter close to the pore size of the support and of variable length. Based on TEM observations, the different outcome of the oxide deposition process can be reasonably attributed to two main factors. (*i*) Different metal oxide loading, leading to the formation of large nanoparticles on the outside surface of SBA-15 for the composite at the highest metal oxide loading (35 wt.%). (*ii*) Different Cu/Zn molar ratio (for the same zirconium oxide content), where for the composite at higher Zn content (Cu/Zn = 1.0) the strong affinity between zinc and the silica walls, leading to the formation of an homogeneous nanolayer at the internal surface of the pores and to the lack of clear nanoparticles by TEM [31,40]. Furthermore, when a high Cu content (Cu/Zn = 2.5) is used, particles of elongated shape with a diameter close to the pore size of the support tend to form during the autocombustion process.

The nitrogen adsorption-desorption isotherms of the fresh CZS and CZZS catalysts series are presented in Fig. 4a, where the isotherm for the bare SBA-15 is also reported for comparison. The silica support exhibits a type IV isotherm with a H1 type hysteresis loop, characteristic of a mesoporous material with uniform cylindrical pores open at both ends [58]. The mesoporous character of the solid is preserved after the incorporation of the active phase, as revealed by the type IV shape of the isotherm in all the catalysts. However, the isotherms (especially for CZZS_35_2.5) is found to shift down along the *y*-axis with the increase in metal oxide loading. This is clearly characteristic of a decrease
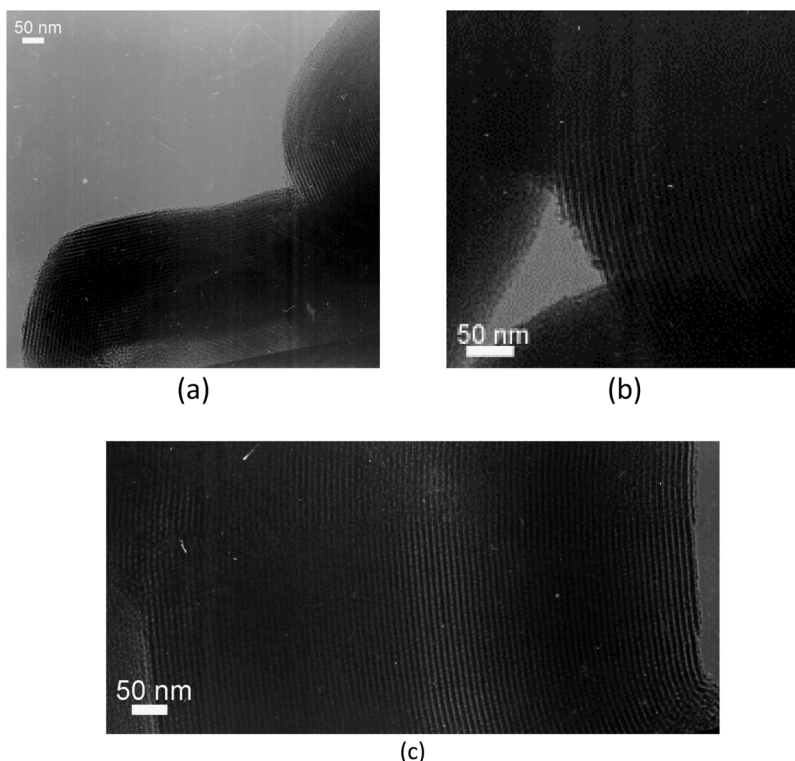

(a)

(b)

(c)

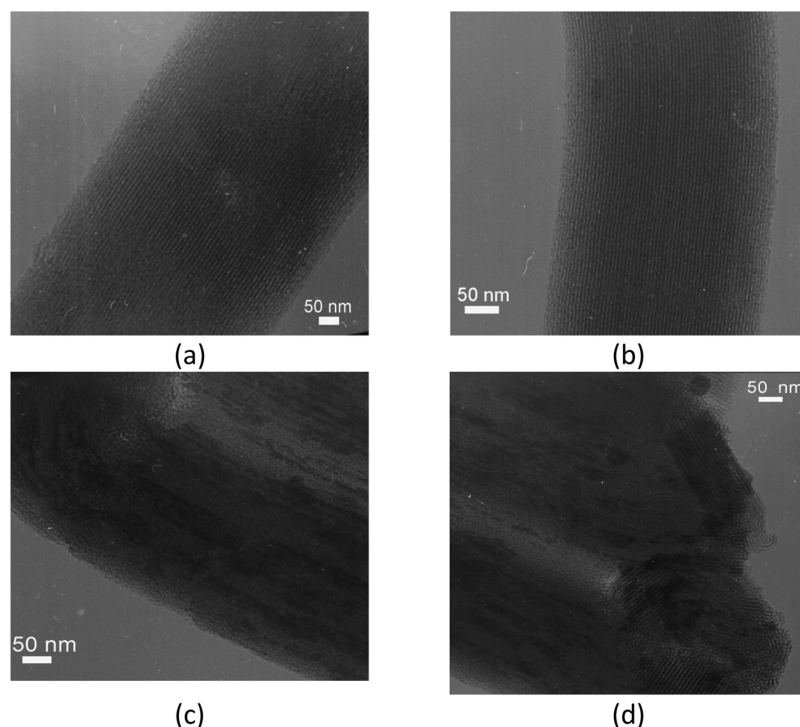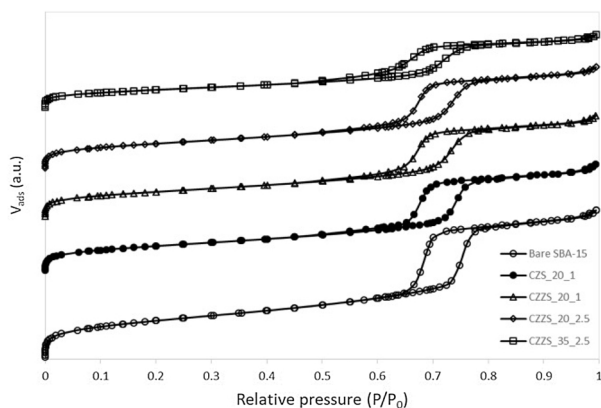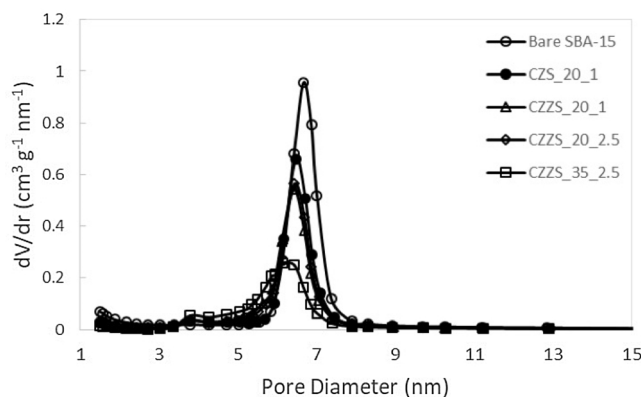**Fig. 2.** TEM images of the CZZS_20_1 catalyst.

Fig. 3. TEM images of the CZZS_35_2.5 catalyst.

(a)

(b)

Fig. 4. Nitrogen adsorption-desorption isotherms (a) and pore size distributions of bare SBA-15 and fresh CZS and CZZS catalysts series.

Table 2

N_2 physisorption data of fresh CZS and CZZS catalysts series compared with the bare SBA-15 and the unsupported CZZ catalyst.

Sample	S_{BET} $(m^2 \ g^{-1})$	D_p (nm)	V_p $(cm^3 \ g^{-1})$
Bare SBA-15	643	6.7	1.06
CZS_20_1	447	6.5	0.81
CZZS_20_1	433	6.4	0.73
CZZS_20_2.5	441	6.4	0.74
CZZS_35_2.5	325	6.2	0.53
CZZ	12	–	0.04

S_{BET}: BET Specific Surface Area; V_p: Pore Volume; D_p: Pore Diameter. Relative Standard Deviation: %RSD (S_{BET}) = 2.1%; %RSD (V_p) = 1.1%; %RSD (D_p) = 1.8%.

in pore volume owing to the partial filling of the pores by the metal oxide phase [50]. A slight decrease of the mean pore diameter by the pore-size distribution plots is also revealed (Fig. 4b). This is consistent with the presence of a layer, clusters or small nanoparticles of metal oxide, in line with the XRD and TEM results. The calculated values of the surface area (S_{BET}), pore volume (V_p) and mean pore diameter (D_p) are reported in Table 2. As shown, the surface area and pore volume of SBA-15 support are reduced to some degree after the metal oxide loading, suggesting the active phase has been successfully confined into the mesoporous channels as a result of the "*in-situ* autocombustion procedure". For all the prepared catalysts, S_{BET} and V_p are lower than the corresponding values of the bare support, which indicates partial filling of the mesopores by the metal oxide. The pore volume decreases in the range 24%–50% (from 1.06 to 0.81 and 1.06 to 0.53 $cm^3 \ g^{-1}$, respectively) passing from the bare SBA-15 to the nanocomposites at 20 and 35 wt.% of active phase, respectively. The effect of the addition of zirconium in the catalyst formulation results in a pore volume decrease (from 0.81 to 0.73 for CZS_20_1 and CZZS_20_1, respectively). Nevertheless, variation of the Cu/Zn molar ratio (1 *vs.* 2.5) does not seem to influence the textural properties of the final catalyst, as the S_{BET}, D_p and V_p values are nearly the same. As shown in the same table, the composite at higher metal oxide loading (CZZS_35_2.5) presents a significantly lower surface area and mesopore volume than the bare SBA-

Table 3
Metal properties of Cu/ZnO/ZrO$_2$@SBA-15 catalysts.

Sample	Cu (wt %)	Dispersion (%)	A_{sam} (m_{Cu}^2°/ g_{ctz})	A_{met} (m_{Cu}^2°/ g_{Cu})	D_p (nm)
CZZS_35_2.5	11.7	26.6	20	171	3.9
CZZS_20_1	5.0	47.2	15	304	2.2

15. The increase of the metal oxide loading (from 20 to 35 wt.%) lead to a marked modification of the textural properties; the S_{BET} and V_p values are reduced by half compared to the bare SBA-15.

The above results suggest that "*in-situ* autocombustion synthesis", especially for the samples at 20 wt.%, is appropriate to limit pore plugging, and consequently leads to an enhancement of the active phase reactivity. It is important to note that the surface areas of the supported catalysts are enormously greater than that of the bulk material (unsupported catalyst, CZZ sample) due to the SBA-15 support contribution (Table 2).

Copper surface areas of the Cu/ZnO/ZrO$_2$@SBA-15 catalysts determined by N$_2$O dissociative adsorption and the corresponding metal dispersion are reported in Table 3. Both samples exhibit high values of Cu^0 surface area and dispersion, considerably higher than those of the Cu/SiO$_2$ catalysts synthetized through conventional impregnation [57,59]. It is possible to observe the highest copper dispersion of CZZS_35_2.5 and CZZS_20_1 catalysts compared to literature data [40], even at high active phase loading (CZZS_35_2.5 sample). Metal dispersion shows a descending trend from 47.2% to 26.6% with an increase of the Cu/Zn molar ratio and active phase loading, suggesting a higher tendency toward the formation of a larger Cu^0 cluster. In particular, the CZZS_20_1 material exhibits a copper dispersion (47.2%) which is more than double than that of the corresponding similar catalysts in the "CN106076395A" patent (22.9%); this confirms the improvement obtained through the innovative impregnation-sol-gel autocombustion combined strategy. As shown, the metal surface area referred to grams of copper is really high, contributing to improve the final performance. Finally, the mean particles size of copper (3.9 nm and 2.2 nm for CZZS_35_2.5 and CZZS_20_1, respectively) are in line with XRD findings and provide a clear indication that the active phase nanoparticles are located inside the mesopores of the silica matrix.

The TCD signal in terms of hydrogen consumption from H$_2$-TPR of all the synthesized catalysts is compared in Fig. 5. Since ZnO and ZrO$_2$ are not reduced within the experimental region considered, the profiles are ascribed to the reduction of the copper oxide phase. As observed in Fig. 5, the catalysts display distinct reduction behaviours depending on the metal oxide loading and on the presence of zirconium in the catalyst formulation. The CZZS_35_2.5 catalyst with the highest active phase loading presents two overlapping peaks of hydrogen consumption centred at 180 and 205 °C respectively, with the onset of the reduction process at a temperature of approximately 110 °C. This result suggests

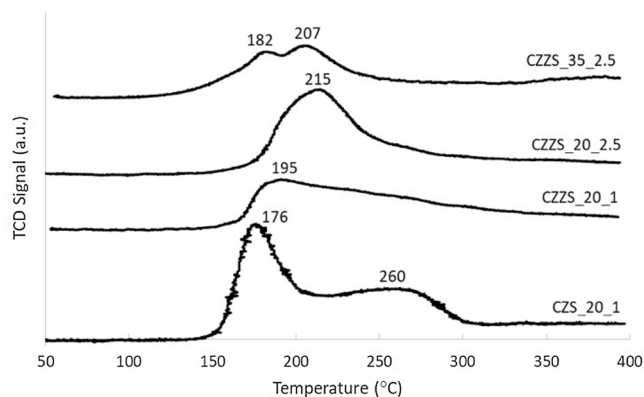**Fig. 5.** H$_2$-TPR profiles of CZS and CZZS catalysts series.

two different types of CuO phases; the first peak at 180 °C is associated with the reduction of highly dispersed CuO species interacting with ZnO and ZrO$_2$ [60–62], whereas the second peak at 205 °C is related to the reduction of bulk-like CuO and/or CuO in big particles (reasonably due to the presence of copper oxide particles on the surface of the SBA-15 support as confirmed by TEM observation) [60,63]. Moreover, the CZZS_20_1 and CZZS_20_2.5 catalysts show only one relative broad peak centred at 190° and 215°, respectively, corresponding to the reduction of CuO to metallic Cu^0 in one step, implying that CuO phase homogeneously dispersed. The amount of consumed H$_2$, calculated from the area under the peaks after calibration of the instrument and referred to the reduction reaction "CuO + H$_2$ → Cu^0 + H$_2$O", is markedly lower than the case of the CZS_20_1 catalyst, supporting the hypothesis of the formation of metallic copper during the "*in-situ* autocombustion synthesis" as observed in the wide-angle XRD patterns. Considering the CZZS_20_1 and CZS_20_1 samples, at the same amount of active phase and with the same Cu/Zn molar ratio, Fig. 5 shows different reduction behaviour and from the results of hydrogen consumption (data not shown) is possible to observe that CZZS_20_1 catalyst needs a lower amount hydrogen indicating a more simple copper reduction. With regard to the zirconium effect, at the same active phase loading (20 wt.%) it is possible to observe a lower temperature reduction of the CZZS catalysts series compared to the CZS one. These results indicate that the ZrO$_2$ phase is able to promote the dispersion of copper oxide and enhances the reducibility of the copper phase; a finding that is consistent with previous observations [23,64–66].

3.2. Catalytic behaviour and post-sorption characterization of the CZS and CZZS composites

The catalytic performance in terms of space time yield and selectivity to methanol for all the catalysts are shown in Fig. 6 and Table 4. Under the conditions of the catalytic tests, the only products of CO$_2$ hydrogenation have been methanol, water and carbon monoxide [67]. According to previous studies [23,68], for copper-based catalysts, well-dispersed CuO particles, Cu surface area and small crystallite size are responsible for the observed catalytic activity. To gain further insight into the relationship between the performance and the properties of the catalysts, several correlations have been built and different effects have been studied, concerning; (*i*) the confinement of the active phase into the SBA-15 mesopores (*ii*) the active phase loading (*iii*) the addition of the zirconia in the formulation of the catalyst (*iv*) the Cu/Zn molar ratio.

Worthy of note is the higher methanol yield per unit mass of the active phase for all the supported catalysts (between 158 and 376 mg$_{CH3OH}$ h^{-1} g$_{cat}^{-1}$), which is much higher than the corresponding value for the unsupported counterpart (10 mg$_{CH3OH}$ h^{-1} g$_{cat}^{-1}$). This suggests that the use of a high surface area support for dispersing on a nanometric scale, the active phase enhances the ability of the latter to catalyse the reaction. On the other hand, a different trend in terms of selectivity to methanol is observed; passing from the unsupported catalyst (CZZ) to the supported ones (CZS and CZZS series), a decrease from 33.3% to 26.4% is observed. This makes it possible to conclude that the effectiveness of the active phase in CO$_2$ hydrogenation to methanol does not depend only on the textural features; a similar behaviour has been already reported by other authors [69].

To the best of the authors' knowledge, nobody has studied the effect of the active phase loading into the mesoporous channels of the SBA-15 on the hydrogenation of CO$_2$ to CH$_3$OH. For this reason, the effect of copper/zinc oxide/zirconium oxide content on SBA-15 (20 and 35 wt. %) on catalytic performance has been further investigated. From Fig. 6b, it can be noted that, with the increase of the active phase loading from 20 to 35 wt.%, there is no improvement in the methanol yield; contrary to what might be expected, this variation leads to a decrease in the activity of the catalyst. According to the XRD and TEM results, this could be due to an increase of the particle size of the active
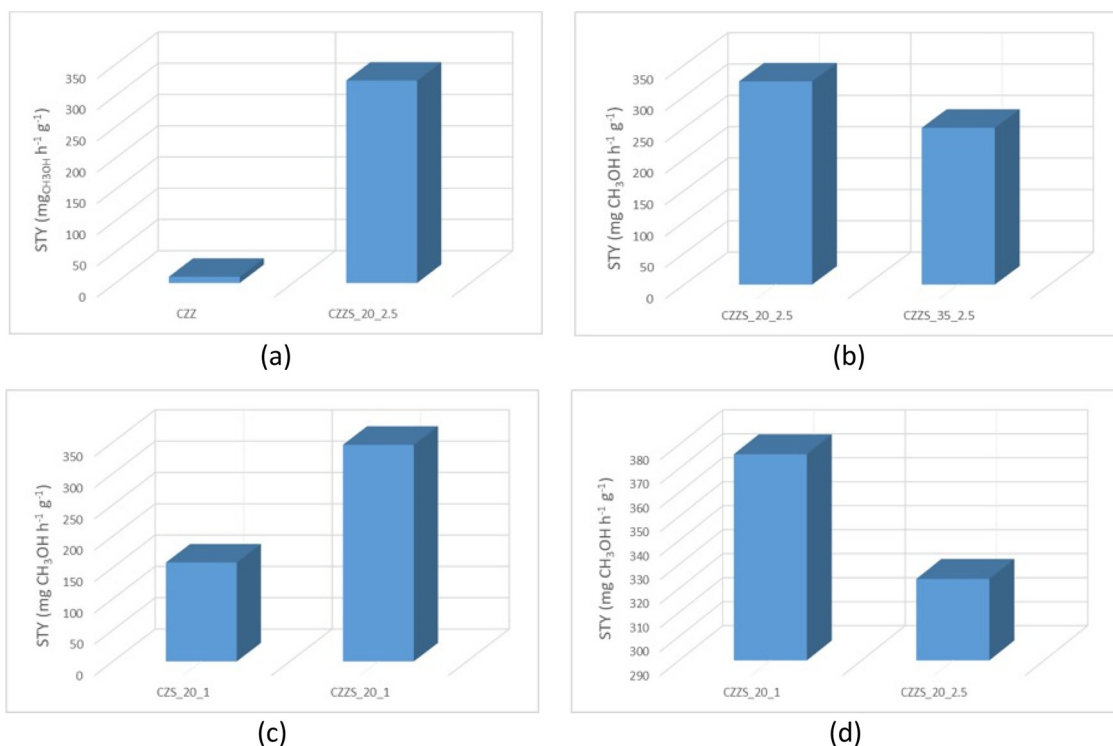
Fig. 6. Catalytic performance of all the prepared catalysts.

Table 4
Catalytic results of the prepared catalysts. Reaction conditions: T $= 250\,°C$; P $= 3.0\,MPa$; $H_2/CO_2 = 3\,mol\,mol^{-1}$; GHSV $= 44,000\,cm^3\,h^{-1}\,g_{cat}^{-1}$; $m_{cat} = 0.45\,g$.

Sample	T.o.S.(h)	S_{CH3OH} (mol %)	STY ($mg_{CH3OH}\,h^{-1}\,g_{cat}^{-1}$)	CO_2 conv.(mol %)
CZS_20_1	68	27.74	158.3	8.9
CZZS_20_1	46	30.60	376.1	19.2
CZZS_20_2.5	31	26.37	324.3	19.1
CZZS_35_2.5	27	24.35	250.2	16.0
CZZ	51	33.31	10.0	0.5

phase as the load increases, resulting in: (*i*) the exposure of a lower number of active sites, and (*ii*) a partial blockage of the pores by copper/zinc oxide/zirconia phases, which would limit or prevent access to the active sites present on the particles deposited inside the SBA-15 channels.

After the addition of zirconium (CZZS_20_1), the methanol yield is noticeably improved compared to those of the binary catalyst (CZS_20_1) showing a more than doubled STY value (376 *vs.* 158 $mg_{CH3OH}\,h^{-1}\,g_{cat}^{-1}$). Moreover, not only does the zirconium-promoted catalyst exhibit a higher methanol yield, but the selectivity to CH_3OH is higher as well (Fig. 7b). Similar findings have been found by some other researcher on ternary Cu-ZnO-ZrO$_2$ catalysts [70].

According to other studies [71], there are two active centres involved in the catalytic process of CO_2 hydrogenation. One is the so-called "active support" whose function is to adsorb CO_2 as carbonate and bicarbonate species, which could undergo stepwise hydrogenation to methanol. The other is the Cu phase, with the purpose of adsorbing H_2 and consequently providing atomic hydrogen to the surface of support by spillover. Such a mechanism is known as a "dual-site" mechanism, and has been recognised by many researchers [64,72,73].

As shown in Fig. 6c, with the same active phase loading (20 wt.%) the Cu/Zn molar ratio only slightly affects the methanol yield and significantly influences the methanol selectivity. Experimental results show that the catalyst with the lowest Cu/Zn molar ratio (1.0 mol
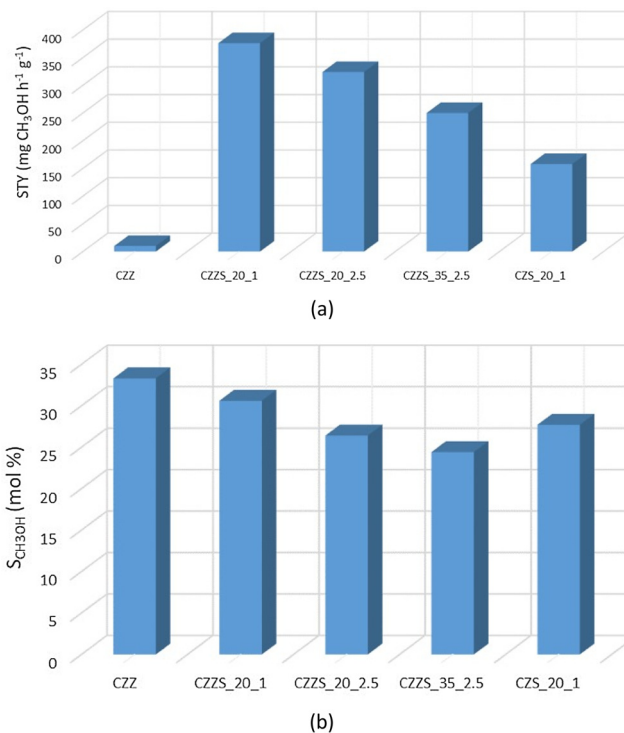

Fig. 7. Comparison of the catalytic performance in terms of space-time-yield (a) and selectivity to methanol (b) of all the prepared catalysts.

mol^{-1}) exhibits the best catalytic performance with a space-time-yield of methanol of 376 $mg_{CH3OH}\,h^{-1}\,g_{cat}^{-1}$. With the increase of the molar ratio to Cu/Zn $= 2.5\,mol\,mol^{-1}$, a slight reduction of methanol productivity to 324 $mg_{CH3OH}\,h^{-1}\,g_{cat}^{-1}$ is observed. From the obtained results, the reduction of the zinc oxide content into the catalyst formulation lead to a worsening of the catalytic performance. A similar outcome in terms of Cu/Zn molar ratio has been found by other

researchers [61]. In other work it has been found that the maximum methanol productivity has been obtained with a Zn/Cu ratio of 0.75 and a decrease of the latter led to a worsening in CO_2 conversion. Such behaviour has been attributed to the strengths between CO_2 molecules (bicarbonate species) and the catalyst surface becoming gradually weaker when the catalysts have been prepared with a higher Zn/Cu ratio. What is clear is the important role that the zinc oxide plays in facilitating the methanol activity as well as the methanol selectivity [74]. These findings further support the idea that no simple correlation exists between the accessibility parameters (S_{BET} and V_p) and the performance of the catalysts, which should be governed by some other features of the material. It is well known that for the Cu-based catalysts for methanol synthesis, the catalytic activity depends greatly on the interaction between Cu and oxide components [75–78]. The intense interaction between Cu and oxide components is in favour of the formation of Cu-MO_x (M = Zn and/or Zr) species which are suggested to exist at the Cu-MO_x interface [79,80]. Evidently, smaller Cu particles can lead to a larger interfacial area of the Cu-MO_x interface, so resulting in higher activity. The obtained achievements of the present work, thus suggest that the interactions between copper and zinc oxide are crucial for the methanol formation. Based on the findings of the present study, the hypothesis can be advanced that interactions of the active phase (especially copper and zinc) are stronger in the CZZS_20_1 catalyst owing to the strong affinity between zinc and the silica walls, leading to the formation of an homogeneous nanolayer at the internal surface of the pores, as observed by TEM micrographs (Fig. 2) and different in terms of crystallinity, particle size and texture from that of the other catalysts. Reasonably, this results in an increasing interaction between copper and zinc oxide. With a higher Cu content (Cu/Zn = 2.5 mol mol^{-1}), the amount of copper interacting with the zinc oxide probably decreases and tends to form particles of elongated shape different from those observed for Cu/Zn = 1.0 mol mol^{-1} (consistent with TEM observation).

Fig. 7a compares the space time yield of methanol for all the prepared catalysts (per mass of active phase). The trend observed parallels that of the methanol yield discussed above, $i.e.$, a maximum activity for the catalyst CZZS_20_1 (with Cu/Zn molar ratio of 1.0 mol mol^{-1}) with a space-time-yield of methanol of 376 mg_{CH3OH} h^{-1} g_{cat}^{-1} which is more than 37-times higher than that of the unsupported CZZ catalyst (10 mg_{CH3OH} h^{-1} g_{cat}^{-1}). The superior performance of the SBA-15 supported catalysts with respect to that of the unsupported can be reasonably ascribed to differences in the exposure of the active phase to the CO_2 and H_2 reactant gas.

Table 5 compares the catalytic systems synthesized and discussed in this work, with the same chemical constituents and, tentatively and obviously, under the same operating conditions (considering the importance of the same, at particular temperature, pressure, and GHSV for productivity in terms of methanol) with the most recent and significant literature data, from which the superior performance of the catalysts, in terms of catalytic efficiency, of the present study are shown.

From Table 5 is possible to observe that all the considered catalysts are exposed to a reactant gas mixture of CO_2/H_2 = 1:3 under a GHSV lower than employed in this work (6600 h^{-1}), except for the CuZnO catalyst prepared by Jeong et al., [81], which uses a GHSV doubled (12,000 h^{-1}). As a result, this latter shows the lowest STY value (0.009 g/g_{cat}/h). In fact, higher GHSV values correspond to lower space time values; generally, this results in a worsening of the final catalytic performance. Therefore, the comparison of the catalytic performance reported in Table 5 is conservative in view that the GHSV used in this work is higher than the others.

The comparison of different studies show how the catalyst developed in this study is more active even at relatively lower working pressures (3.0 MPa), compared to the 5.0 MPa required by the CuO-ZnO/Al_2O_3 catalyst [84] which, although it is the best, reaches far lower values of productivity of methanol.

3.3. Catalysts stability

In general, the activity of a catalyst during operation is one of the key issues in the development of the material. In order to investigate this property, a 30 -h continuous test has been carried out. The analysis of the gas and liquid effluent reveals that only CO, CH_3OH and H_2O (as well as unconverted H_2 and CO_2) are present and no other alcohols or esters have been detected. It is known that thermal, hydrothermal and mechanical stability are key parameters in such a kind of application. SBA-15 has been deliberately selected because their peculiar features, among which its thick pore walls (2–6 nm), leading to improved thermal and hydrothermal stability compared to other M41S materials; the latter show poor hydrothermal stability in presence of water due to the hydrolysis of the silicate groups constituting the amorphous silica pore walls that result thin [86,87]. On the contrary, SBA-15 is able to tolerate severe treatment with vapour in presence of autogenous pressure at 100 °C (100% of moisture), [88]. As expected, the results for the unsupported CZZ catalyst reveal a very poor time-on-stream activity, as a consequence of the restricted exposure of the active phase to the CO_2 and H_2. The stability of all the supported catalysts in terms of space-time yield (Fig. 8a) shows a slight decrease in range from 5 to 14% during the 25 h time-on-stream experiment. The CZZS_20_1 composite exhibits the highest methanol productivity together with the lowest STY variation (5%), whereas a more remarkable reduction is observed for the CZZS_35_2.5 and CZS_20_1 catalysts (11 and 14%, respectively). The latter may be ascribable to the agglomerate or sintering of copper particles, as has already been observed by several authors for similar materials [69,89,90]. This behaviour can be directly correlated to the findings of XRD, TEM and N_2-physisorption data; as previously reported, the confinement of a high active phase content (35 wt.%) leads to the formation of large nanoparticles on the outside surface of SBA-15 that can in turn sinter or agglomerate during the reaction, causing a reduction of methanol activity. With regard to the CZS_20_1 composite, this behaviour can be reasonably attributed to the absence of the

Table 5
Comparison of the catalytic data obtained for the most promising catalyst synthesized with the most significant catalysts reported in the most recent literature.

Catalyst	STY (MeOH) (g/g_{cat}/h)	(T - P) (°C, MPa)	GHSV (h^{-1})	Reference
Cu-ZnO/Al_2O_3	0.011	250 - 2.0	1400-5000	Ren et al., 2015 [82]
Cu-ZnO	0.009	250 - 3.0	12,000	Jeong et al., 2012 [81]
Cu-Zn-Ga	0.135	270 - 3.0	3000	Cai et al., 2015 [83]
CuO-ZnO/Al_2O_3	0.10	250 - 3.0	3600	Tursunov et al., 2017 [84]
	0.06			
CuO-ZnO/SiO_2	0.07	250 - 5.0	3600	Tursunov et al., 2017 [84]
	0.05			
CuO-ZnO/SiO_2	0.06	250 - 3.0	3600	Tursunov et al., 2017 [84]
	0.045			
Cu/ZnO-SBA-15 (CZS_20_1)	**0.158**	250 - 3.0	6600	This work
Cu/ZnO/ZrO_2	0.210	270 - 5.0	4600	Dong et al., 2016 [85]
Cu/ZnO/ZrO_2-SBA-15 (CZZS_20_1)	**0.376**	250 - 3.0	6600	This work

(a)

(b)

(c)
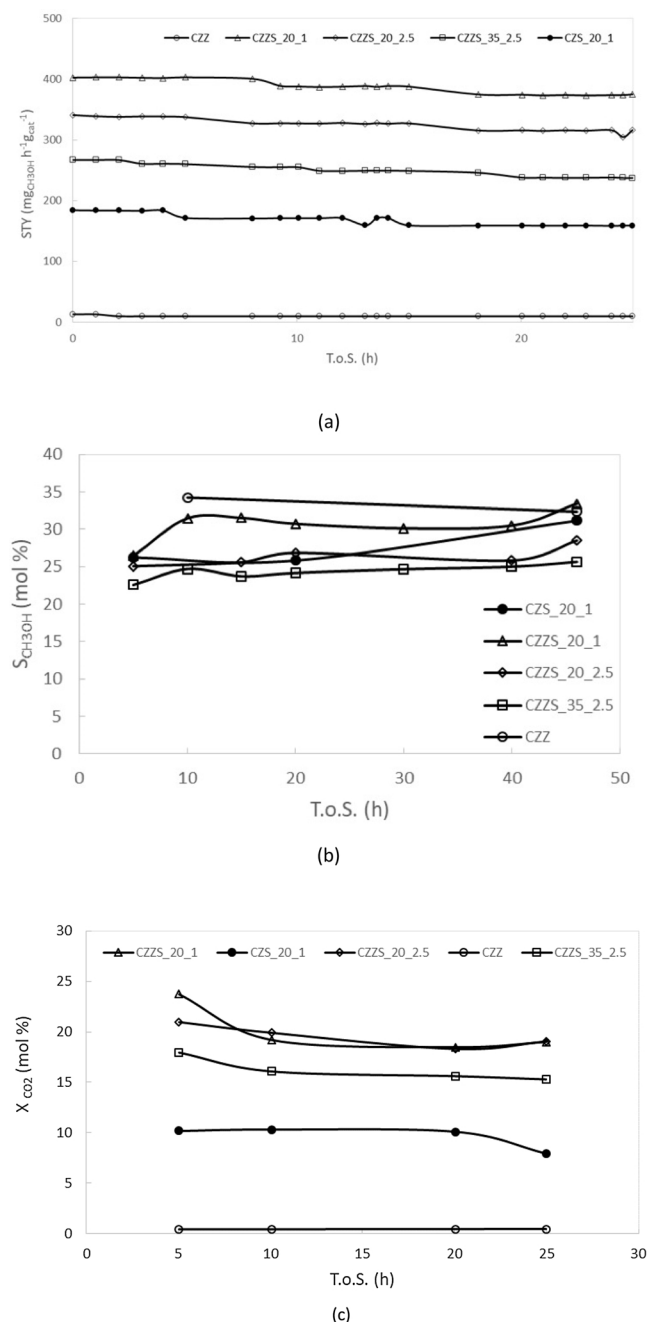
Fig. 8. Space-time yield (a), selectivity (b) and CO_2 conversion (c) of methanol as a function of time-on-stream of CZS and CZZS catalysts series. Result for the unsupported CZZ catalyst is also reported for comparison. Reaction conditions: T $= 250\,°C$; P $= 3.0\,MPa$; $H_2/CO_2 = 3\,mol\;mol^{-1}$; GHSV $= 44,000\;cm^3\;g_{cat}^{-1}\,h^{-1}$; $m_{cat} = 0.45\,g$.

Table 6
N_2 physisorption data of the fresh and used CZZS_20_1 catalyst.

Sample	$S_{BET}\;(m^2\;g^{-1})$	$D_p\;(nm)$	$V_p\;(cm^3\;g^{-1})$
CZZS_20_1_Fresh	433	6.4	0.73
CZZS_20_1_Used	425	6.4	0.73

S_{BET}: BET Specific Surface Area; V_p: Pore Volume; D_p: Pore Diameter. Relative Standard Deviation: %RSD (S_{BET}) = 2.1%; %RSD (V_p) = 1.1%; %RSD (D_p) = 1.8%.

zirconia in the catalyst formulation, resulting in a lower dispersion of copper oxide. At variance with the case of CZZS_35_2.5 and CZS_20_1, the higher stability of the CZZS_20_1 catalyst could be attributed to the higher dispersion of the active phase on the SBA-15 and the stronger metal-support interaction which could prevent the restructuring effects of copper particles [69]. This hypothesis is further supported by the XRD and TEM results, where the deposition of an amorphous active phase thin layer at the surface of the SBA-15 channels has been postulated. Such a finding not only makes the active phase more available to the reaction between hydrogen and carbon dioxide, but also prevents the sintering or agglomeration of the active phase particles. To get further clues to the proposed occurrence, the textural properties of the CZZS_20_1 catalyst after 50 h of continuous reaction have been investigated and the pertinent results are shown in Table 6. After the catalytic run, the support mesostructure is retained. Comparison of the S_{BET}, D_p and V_p values of the used catalyst with those for the corresponding fresh catalyst confirm that all the textural parameters remain unchanged.

As reported in Fig. 8b the methanol selectivity for the CZS and CZZS catalysts series does not show any decline during the test period, indicating remarkable stability; on the other hand, only the unsupported CZZ catalyst shows a slight decrease of methanol selectivity. Similar trend is found for the CO_2 conversion and no appreciable decreasing during time-on-stream is observed. Nevertheless, a difference between the catalyst CZZS_20_1 and CZZS_20_2.5 with the same active phase loading is possible to observe compared to that reported in Fig. 8a. Although the CO_2 conversion of these catalysts appears to be similar, a difference in terms of methanol productivity (Fig. 8a) is observable; this can be reasonably attributed to the higher methanol selectivity of the CZZS_20_1 compared to the CZZS_20_2.5. Moreover, this indicates that a lower Cu/Zn molar ratio - with the same active phase content - positively affects the methanol selectivity, which in turn enhances the space time yield of methanol.

The low-angle diffraction pattern of the used CZZS_20_1 catalyst shows that the characteristic hexagonal order is preserved (Fig. 9a). Only a slight shift towards higher angles as compared to that of the fresh pattern, suggesting a slight shrinkage in the mesoporous framework. The wide-angle XRD pattern of the used catalyst (Fig. 9b) show that for the used sample, in addition to the broad halo related to amorphous silica, a low intensity diffraction peak at $2\Theta = ca.\;43.2°$ assigned to the metallic copper phase (PDF Card 4-0836).

4. Conclusions

Copper/zinc oxide/zirconium oxide@SBA-15 composites with good performance for methanol synthesis from CO_2 hydrogenation have been synthesized by an innovative combined impregnation-solgel auto-combustion approach with different active phase loading (20 and 35 wt. %) and Cu/Zn molar ratio (1.0 and 2.5 mol mol^{-1}). Subsequent characterization of the nanocatalysts clearly showed that the synthesis procedure is efficient in obtaining nanometric particles, even if a difference in terms of active phase crystallinity and dispersion has been observed from the XRD and TEM results. A remarkable space time yield of methanol referring to the active phase is shown; at variance with the case of the unsupported catalyst (10 $mg_{CH3OH}\;h^{-1}\;g_{cat}^{-1}$), the methanol yield 37-fold higher is shown for the supported catalyst (376 $mg_{CH3OH}\;h^{-1}\;g_{cat}^{-1}$) with a Cu/Zn molar ratio of 1.0 mol mol^{-1} and a total active phase loading of 20 wt.%. Based on the obtained results, the methanol yield and methanol selectivity are strongly influenced by: (*i*) the active phase loading and the copper/zinc molar ratio leading to differences in the morphology and dispersion of the active phase, which in turn cause the composite to catalyse the reaction differently; (*ii*) the presence of zirconia that enhances both the yield and selectivity to methanol by approximately 58% and 9.5%, respectively. Better results have been found when a thin amorphous homogeneous layer of the active phase is formed, rather than elongated particles with a diameter close to those
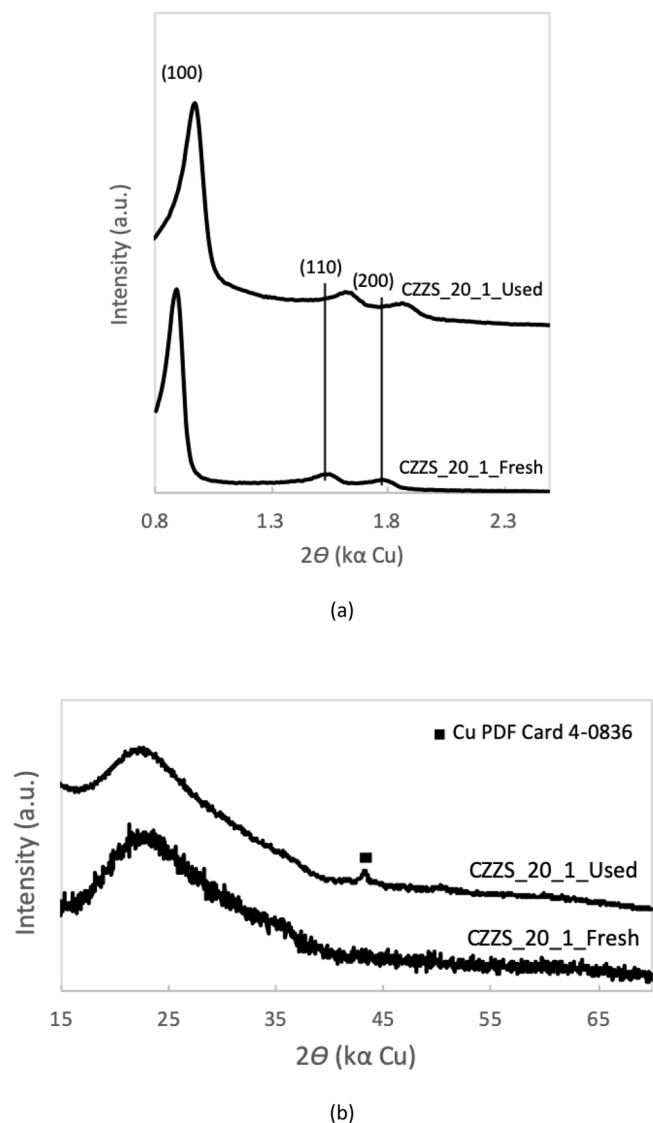
(a)

(b)

Fig. 9. XRD patterns of fresh and used CZZS_20_1 catalyst at low-angle (a) and wide-angle (b). The main reflection plane is marked.

of the mesochannels or bigger particles located at the external surface; the first finding has led to the enhancement of the interaction among the various single active phases which in turn determine an improvement in terms of activity and selectivity of the catalyst.

The results of 50 h of continuous reaction revealed high performance and steady stability of these systems, especially for CZZS_20_1 catalyst.

Declarations of Competing Interest

The authors declare that they have no known competing financial interests or personal relationships that could have appeared to influence the work reported in this paper.

Acknowledgements

References

[1] M. Bui, C.S. Adjiman, A. Bardow, E.J. Anthony, A. Boston, S. Brown, P.S. Fennell, S. Fuss, A. Galindo, L.A. Hackett, J.P. Hallett, H.J. Herzog, G. Jackson, J. Kemper, S. Krevor, G.C. Maitland, M. Matuszewski, I.S. Metcalfe, C. Petit, G. Puxty, J. Reimer, D.M. Reiner, E.S. Rubin, S.A. Scott, N. Shah, B. Smit, J.P.M. Trusler, P. Webley, J. Wilcox, N. Mac Dowell, Carbon capture and storage (CCS): the way forward, Energy Environ. Sci. 11 (2018) 1062–1176.

[2] T.M. Gür, Review of electrical energy storage technologies, materials and systems: challenges and prospects for large-scale grid storage, Energy Environ. Sci. 11 (2018) 2696–2767.

[3] A. Rafiee, K.R. Khalilpour, D. Milani, CO_2 conversion and utilization pathways, in: K.R. Khalilpour (Ed.), Polygeneration With Polystorage for Chemical and Energy Hubs For Energy and Chemicals, Elsevier Academic Press, London (United Kingdom), 2019, pp. 213–245 chapter 8.

[4] E.I. Koytsoumpa, C. Bergins, E. Kakaras, The CO_2 economy: review of CO_2 capture and reuse technologies, J. Supercrit. Fluids 132 (2018) 3–16.

[5] A. Otto, T. Grube, S. Schiebahn, D. Stolten, Closing the loop: captured CO_2 as a feedstock in the chemical industry, Energy Environ. Sci. 8 (2015) 3283–3297.

[6] J.C. Abanades, E.S. Rubin, M. Mazzotti, H.J. Herzog, On the climate change mitigation potential of CO_2 conversion to fuels, Energy Environ. Sci. 10 (2017) 2491–2499.

[7] H.A. Daggash, C.F. Patzschke, C.F. Heuberger, L. Zhu, K. Hellgardt, P.S. Fennell, A.N. Bhave, A. Bardow, N. Mac Dowell, Closing the carbon cycle to maximise climate change mitigation: power-to-methanol vs. power-to-direct air capture, Sustainable Energy Fuels 2 (2018) 1153–1169.

[8] M.D. Porosoff, B. Yan, J.G. Chen, Catalytic reduction of CO_2 by H_2 for synthesis of CO, methanol and hydrocarbons: challenges and opportunities, Energy Environ. Sci. 9 (2016) 62–73.

[9] M. Meng-Jung, Li, S. Chi Edman Tsang, Bimetallic catalysts for green methanol production via CO2 and renewable hydrogen: a mini-review and prospects, Catal. Sci. Technol. 8 (2018) 3450–3464.

[10] J.M. Thomas, K.D.M. Harris, Some of tomorrow's catalysts for processing renewable and non-renewable feedstocks, diminishing anthropogenic carbon dioxide and increasing the production of energy, Energy Environ. Sci. 9 (2016) 687–708.

[11] X. Zhang, L. Zhong, Q. Guo, H. Fan, H. Zheng, K. Xie, Influence of the calcination on the activity and stability of the $Cu/ZnO/Al_2O_3$ catalyst in liquid phase methanol synthesis, Fuel 89 (2010) 1348–1352.

[12] E. Kleymenov, J. Sa, J. Abu-Dahrieh, D. Rooney, J.A. van Bokhoven, E. Troussard, J. Szlachetko, O.V. Safonova, M. Nachtegaal, Structure of the methanol synthesis catalyst determined by in situ HERFD XAS and EXAFS, Catal. Sci. Technol. 2 (2012) 373–378.

[13] C. Baltes, S. Vukojević, F. Schüth, Correlations between synthesis, precursor, and catalyst structure and activity of a large set of $CuO/ZnO/Al_2O_3$ catalysts for methanol synthesis, J. Catal. 258 (2008) 334–344.

[14] I. Kasatkin, P. Kurr, B. Kniep, A. Trunschke, R. Schlögl, Role of lattice strain and defects in copper particles on the activity of $Cu/ZnO/Al_2O_3$ catalysts for methanol synthesis, Angew. Chem. 119 (2007) 7465–7468.

[15] Y. Zhang, Q. Sun, J. Deng, D. Wu, S. Chen, A high activity $Cu/ZnO/Al_2O_3$ catalyst for methanol synthesis: preparation and catalytic properties, Appl. Catal. A Gen. 158 (1997) 105–120.

[16] G. Chinchen, P. Denny, J. Jennings, M. Spencer, K. Waugh, Synthesis of methanol: Part 1. Catalysts and kinetics, Appl. Catal. 36 (1998) 1–65.

[17] J.L. Li, T. Inui, Enhancement in methanol synthesis activity of a copper/zinc/aluminum oxide catalyst by ultrasonic treatment during the course of the preparation procedure, Appl. Catal. A Gen. 139 (1996) 87–96.

[18] J.S. Lee, K.H. Lee, S.Y. Lee, Y.G. Kim, A comparative study of methanol synthesis from CO_2/H_2 and CO/H_2 over a $Cu/ZnO/Al_2O_3$ catalyst, J. Catal. 144 (1993) 414–424.

[19] G. Wang, D. Mao, X. Guo, J. Yu, Methanol synthesis from CO_2 hydrogenation over CuO-ZnO-ZrO2-MxOy catalysts (M = Cr, Mo and W), Int. J. Hydrogen Energy 44 (2019) 4197–4207.

[20] G. Bonura, M. Cordaro, C. Cannilla, F. Arena, F. Frusteri, The changing nature of the active site of Cu-Zn-Zr catalysts for the CO_2 hydrogenation reaction to methanol, Appl. Catal. B 152-153 (2014) 152–161.

[21] R. Ladera, F.J. Pérez-Alonso, J.M. González-Carballo, M. Ojeda, S. Rojas, J.L.G. Fierro, Catalytic valorization of CO_2 via methanol synthesis with Ga-promoted Cu–ZnO–ZrO2 catalysts, Appl. Catal. B 142–143 (2013) 241–248.

[22] F. Arena, G. Mezzatesta, G. Zafarana, G. Trunfio, F. Frusteri, L. Spadaro, Effects of oxide carriers on surface functionality and process performance of the Cu–ZnO system in the synthesis of methanol via CO_2 hydrogenation, J. Catal. 300 (2013) 141–151.

[23] X. Guo, D. Mao, G. Lu, S. Wang, G. Wu, Glycine-nitrate combustion synthesis of CuO–ZnO–ZrO2 catalysts for methanol synthesis from CO_2 hydrogenation, J. Catal. 271 (2010) 178–185.

[24] R. Raudaskoski, M.V. Niemelä, R.L. Keiski, The effect of ageing time on co-precipitated $Cu/ZnO/ZrO_2$ catalysts used in methanol synthesis from CO_2 and H_2, Top. Catal. 45 (2007) 57–60.

[25] J. Słoczyński, R. Grabowski, P. Olszewski, A. Kozłowska, J. Stoch, M. Lachowska, J. Skrzypek, Effect of metal oxide additives on the activity and stability of $Cu/ZnO/ZrO_2$ catalysts in the synthesis of methanol from CO_2 and H_2, Appl. Catal. A Gen.

310 (2006) 127–137.

[26] J. Wang, G. Li, Z. Li, C. Tang, Z. Feng, H. An, H. Liu, T. Liu, C. Li, A highly selective and stable ZnO-ZrO$_2$ solid solution catalyst for CO$_2$ hydrogenation to methanol, Sci. Adv. 3 (2017) e1701290.

[27] C.H. Bartholomew, Mechanisms of catalyst deactivation, Appl. Catal. A Gen. 212 (2001) 17–60.

[28] M.V. Twigg, M.S. Spencer, Deactivation of copper metal catalysts for methanol decomposition, methanol steam reforming and methanol synthesis, Top. Catal. 22 (2003) 191–203.

[29] H.H. Kung, Deactivation of methanol synthesis catalysts – a review, Catal. Today 11 (1992) 443–453.

[30] J. Wu, M. Saito, M. Takeuchi, T. Watanabe, The stability of Cu/ZnO-based catalysts in methanol synthesis from a CO$_2$-rich feed and from a CO-rich feed, Appl. Catal. A Gen. 218 (2001) 235–240.

[31] M. Mureddu, I. Ferino, A. Musinu, A. Ardu, E. Rombi, M.G. Cutrufello, P. Deiana, M. Fantauzzi, C. Cannas, MeOx/SBA-15 (Me = Zn, Fe): highly efficient nanosorbents for mid-temperature H2S removal, J. Mater. Chem. A Mater. Energy Sustain. 2 (2014) 19396–19406.

[32] L. Wang, L. Yang, Y. Zhang, W. Ding, S. Chen, W. Fang, Y. Yang, Promoting effect of an aluminum emulsion on catalytic performance of Cu-based catalysts for methanol synthesis from syngas, Fuel Process. Technol. 91 (2010) 723–728.

[33] F.H. Tasfy, N.A.M. Zabidi, M. Shima Shaharun, D. Subbarao, . The Role of Support Morphology on the Performance of Cu/ZnO-Catalyst for Hydrogenation of CO$_2$ to Methanol, Proceeding of 23rd Scientific Conference of the Microscopy Society Malaysia 2014 (SCMSM2014), (2014) December.

[34] D. Zhao, J. Feng, Q. Huo, N. Melosh, G.H. Fredrikson, B.F. Chmelka, G.D. Stucky, Triblock copolymer syntheses of mesoporous silica with periodic 50 to 300 angstrom pores, Science 279 (1998) 548–552.

[35] C. Rudolf, F. Abi-Ghaida, B. Dragoi, A. Ungureanu, A. Mehdi, E. Dumitriu, An efficient route to prepare highly dispersed metallic copper nanoparticles on ordered mesoporous silica with outstanding activity for hydrogenation reactions, Catal. Sci. Technol. 5 (2015) 3735–3745.

[36] B. Dragoi, I. Mazilu, A. Chirieac, C. Ciotonea, A. Ungureanu, E. Marceau, E. Dumitriu, S. Royer, Highly dispersed copper (oxide) nanoparticles prepared on SBA-15 partially occluded with the P123 surfactant: toward the design of active hydrogenation catalysts, Catal. Sci. Technol. 7 (2017) 5376–5385.

[37] S. Karthikeyan, M.P. Pachamuthu, Mark A. Isaacs, Santosh Kumar, Adam F. Lee, G. Sekaran, Cu and Fe oxides dispersed on SBA-15: a Fenton type bimetallic catalyst for N,N-diethyl-p-phenyl diamine degradation, Appl. Catal. B 199 (2016) 323–330.

[38] Y. Sun, S. Walspurger, J.P. Tessonnier, B. Louis, J. Sommer, Highly dispersed iron oxide nanoclusters supported on ordered mesoporous SBA-15: a very active catalyst for Friedel–crafts alkylations, Appl. Catal. A Gen. 300 (2000) 1–7.

[39] G. Prieto, A. Martínez, R. Murciano, M.A. Arribas, Cobalt supported on morphologically tailored SBA-15 mesostructures: the impact of pore length on metal dispersion and catalytic activity in the Fischer–tropsch synthesis, Appl. Catal. A Gen. 367 (2009) 146–156.

[40] A. Garcia-Trenco, A. Martinez, A simple and efficient approach to confine Cu/ZnO methanol synthesis catalysts in the ordered mesoporous SBA-15 silica, Catal. Today 215 (2013) 152–161.

[41] S.F.H. Tasfy, N.A.M. Zabidi, M.S. Shaharun, D. Subbarao, The influence of Mn, Zr and Pb promoters on the performance of Cu/ZnO/SBA-15 catalyst for hydrogenation of CO$_2$ to methanol, Defect Diffus. Forum 365 (2015) 178–182.

[42] S.F.H. Tasfy, N.A.M. Zabidi, M.S. Shaharun, D. Subbarao, A. Elbagir, Carbon dioxide hydrogenation to methanol over Cu/ZnO-SBA-15 catalyst: effect of metal loading, Defect Diffus. Forum 380 (2017) 151–160.

[43] A.J. van Dillen, R.J.A.M. Terörde, D.J. Lensveld, J.W. Geus, K.P. de Jong, Synthesis of supported catalysts by impregnation and drying using aqueous chelated metal complexes, J. Catal. 216 (2003) 257–264.

[44] N. Kotter, L. Riekert, The influence of impregnation, drying and activation on the activity and distribution of CuO on α-Alumina, Stud. Surf. Sci. Catal. 3 (1979) 51–63.

[45] J.W. Geus, J.A.R. van Veen, Catalysis. An integrated approach, in: R.A. van Santen, P.W.N.M. van Leeuwen, J.A. Moulijn, B.A. Averill (Eds.), Second Revised and Enlarged Edition, Elsevier, Amsterdam, 1999, p. 459.

[46] L.M. Knijff, The application of active components into catalyst support bodies, Ph.D. Thesis, Utrecht University, Utrecht, The Netherlands, 1993.

[47] D.J. Lensveld, J.G. Mesu, A.J. Van Dillen, K.P. De Jong, Synthesis and characterisation of MCM-41 supported nickel oxide catalysts, Microporous Mesoporous Mater. 44-45 (2001) 401–407.

[48] P.J. Van den Brink, A. Scholten, A. Van Wageningen, M.D.A. Lamers, A.J. Van Dillen, J.W. Geus, The use of chelating agents for the preparation of iron oxide catalysts for the selective oxidation of hydrogen sulfide, Stud. Surf. Sci. Catal. 63 (1991) 527–536.

[49] A. Infantes-Molina, J. Merida-Robles, P. Braos-Garcia, E. Rodriguez-Castellon, E. Finocchio, G. Busca, P. Maireles-Torres, A. Jimenez-Lopez, Nickel supported on porous silica as catalysts for the gas-phase hydrogenation of acetonitrile, J. Catal. 225 (2004) 479–488.

[50] X. Zhong, J. Barbier Jr., D. Duprez, H. Zhang, S. Royer, Modulating the copper oxide morphology and accessibility by using micro-/mesoporous SBA-15 structures as host support: effect on the activity for the CWPO of phenol reaction, Appl. Catal. B 121-122 (2012) 123–134.

[51] D. Sellam, M. Bonne, S. Arrii-Clacens, G. Lafaye, N. Bion, S. Tezkratt, S. Royer, P. Marécot, D. Duprez, Simple approach to prepare mesoporous silica supported mixed-oxide nanoparticles by in situ autocombustion procedure, Catal. Today 157 (2010) 131–136.

[52] L. Xiang, S. Royer, H. Zhang, J.-M. Tatibouët, J. Barrault, S. Valange, Properties of iron-based mesoporous silica for the CWPO of phenol: a comparison between impregnation and co-condensation routes, J. Hazard. Mater. 172 (2009) 1175–1184.

[53] Y. Narendar, G.L. Messing, Mechanism of phase separation in gel-based synthesis of multicomponent metal oxides, Catal. Today 35 (1997) 247–268.

[54] S.R. Jain, K.C. Adiga, V.R. Pai Verneker, A new approach to thermochemical calculations of condensed fuel-oxidizer mixture, Combust. Flame 40 (1981) 71–79.

[55] H.P. Klug, L.E. Alexander, X-Ray Diffraction Procedures: For Polycrystalline and Amorphous Materials, John Wiley & Sons, Inc., New York, 1954, pp. 491–538 ch. 9.

[56] E.P. Barret, L.G. Joyner, P.P. Halenda, The determination of pore volume and area distributions in porous substances. I. Computations from nitrogen isotherms, J. Am. Chem. Soc. 73 (1951) 373–380.

[57] A. Gervasini, S. Bennici, Dispersion and surfaces states of copper catalysts by temperature programmed reduction of oxidized surfaces (s TPR), Appl. Catal. A Gen. 281 (2005) 199–205.

[58] F. Rouquerol, J. Rouquerol, K. Sing, Adsorption by Powders and Porous Solids, Elsevier Academic Press, 1999, pp. 191–217 ch. 7.

[59] G.C. Bond, S.N. Namijo, An improved procedure for estimating the metal surface area of supported copper catalysts, J. Catal. 118 (1989) 507–510.

[60] H. Lei, Z. Hou, J. Xie, Hydrogenation of CO$_2$ to CH$_3$OH over CuO/ZnO/Al$_2$O$_3$ catalysts prepared via a solvent-free routine, Fuel 164 (2016) 191–198.

[61] T. Witoon, N. Kachaban, W. Donphai, P. Kidkhunthod, K. Faungnawakij, M. Chareonpanich, J. Limtrakul, Tuning of catalytic CO$_2$ hydrogenation by changing composition of CuO-ZnO ZrO$_2$ catalysts, Energy Convers. Manage. 118 (2016) 21–31.

[62] Y. Zhang, J. Fei, Y. Yu, X. Zheng, Methanol synthesis from CO$_2$ hydrogenation over Cu based catalyst supported on zirconia modified γ-Al$_2$O$_3$, Energy Convers. Manage. 47 (2006) 3360–3367.

[63] L.C. Wang, Y.M. Liu, M. Chen, Y. Cao, H.Y. He, G.S. Wu, W.L. Dai, K.N. Fan, Production of hydrogen by steam reforming of methanol over Cu/ZnO catalysts prepared via a practical soft reactive grinding route based on dry oxalate-precursor synthesis, J. Catal. 246 (193) (2007) 204.

[64] J. Xiao, D. Mao, X. Guo, J. Yu, Effect of TiO$_2$, ZrO$_2$, and TiO$_2$-ZrO$_2$ on the performance of CuO-ZnO catalyst for CO$_2$ hydrogenation to methanol, Appl. Surf. Sci. 338 (2015) 146–153.

[65] N.F.P. Ribeiro, M.M.V.M. Souza, M. Schmal, Combustion synthesis of copper catalysts for selective CO oxidation, J. Power Sources 179 (2008) 329–334.

[66] L.C. Wang, Q. Liu, M. Chen, Y.M. Liu, Y. Cao, H.Y. He, K.N. Fan, Structural evolution and catalytic properties of nanostructured CuZrO$_2$ catalysts prepared by oxalate gel-coprecipitation technique, J. Phys. Chem. C. 111 (2007) 16549–16557.

[67] J. Słoczyński, R. Grabowski, A. Kozłowska, P. Olszewski, J. Stoch, J. Skrzypek, M. Lachowska, Catalytic activity of the M/(3ZnO.ZrO$_2$) system (M = Cu, Ag, Au) in the hydrogenation of CO$_2$ to methanol, Appl. Catal. A Gen. 278 (2004) 11–23.

[68] G. Avgouropoulos, T. Ioannides, H. Matralis, Influence of the preparation method on the performance of CuO–CeO$_2$ catalysts for the selective oxidation of CO, Appl. Catal. B 56 (2005) 87–93.

[69] T. Witoon, J. Chalorngtham, P. Dumrongbunditkul, M. Chareonpanich, J. Limtrakul, CO$_2$ hydrogenation to methanol over Cu/ZrO$_2$ catalysts: effects of zirconia phases, Chem. Eng. J. 293 (2016) 327–336.

[70] Y. Wang, S. Kattel, W. Gao, K. Li, P. Liu, J.G. Chen, H. Wang, Exploring the ternary interactions in Cu-ZnO-ZrO$_2$ catalysts for efficient CO$_2$ hydrogenation to methanol, Nat. Commun. 10 (2019) 1166.

[71] I.A. Fisher, A.T. Bell, In-situ infrared study of methanol synthesis from H$_2$/CO$_2$ over Cu/SiO$_2$ and Cu/ZrO$_2$/SiO$_2$, J. Catal. 172 (1997) 222–237.

[72] X.M. Guo, D.S. Mao, G.Z. Lu, S. Wang, G.S. Wu, The influence of La doping on the catalytic behavior of Cu/ZrO$_2$ for methanol synthesis from CO$_2$ hydrogenation, J. Mol. Catal. A Chem. 345 (2011) 60–68.

[73] F. Arena, G. Mezzatesta, G. Zafaana, G. Trunfio, F. Frusteri, L. Spadaro, How oxide carriers control the catalytic functionality of Cu-ZnO system in the hydrogenation of CO$_2$ to methanol, Catal. Today 210 (2013) 39–46.

[74] S.F.H. Tasfy, N.A.M. Zabidi, M.S. Shaharun, Hydrogenation of CO$_2$ to methanol over copper-zinc oxide based catalyst, Int. J. Chem., Mol., Nuclear, Mater. Metall. Eng. 11 (2017) 108–113.

[75] T. Witoon, T. Permsirivanich, W. Donphai, A. Jaree, M. Chareonpanich, CO$_2$ hydrogenation to methanol over Cu/ZnO nanocatalysts prepared via a chitosan-assisted co-precipitation method, Fuel Process. Technol. 116 (2013) 72–78.

[76] Q. Sun, Y.L. Zhang, H.Y. Chen, J.F. Deng, D. Wu, S.Y. Chen, A novel process for the preparation of Cu/ZnO and Cu/ZnO/Al$_2$O$_3$ ultrafine catalyst: structure, surface properties, and activity for methanol synthesis from CO$_2$ + H$_2$, J. Catal. 167 (1997) 92–105.

[77] D.J. Wang, J. Zhao, H.L. Song, L.J. Chou, Characterization and performance of Cu/ZnO/Al$_2$O$_3$ catalysts prepared via decomposition of M(Cu, Zn)-ammonia complexes under sub-atmospheric pressure for methanol synthesis from H$_2$ and CO$_2$, J. Nat. Gas Chem. 20 (2011) 629–634.

[78] L. Li, D. Mao, J. Yu, X. Guo, Highly selective hydrogenation of CO$_2$ to methanol over CuO-ZnO-ZrO$_2$ catalysts prepared by a surfactant-assisted coprecipitation method, J. Power Sources 279 (2015) 394–404.

[79] J.D. Grunwaldt, A.M. Molenbroek, N.Y. Topsøe, H. Topsøe, B.S. Clausen, In situ investigations of structural changes in Cu/ZnO catalysts, J. Catal. 194 (2000) 452–460.

[80] F.L. Liao, Z.Y. Zeng, C. Eley, Q. Lu, X.L. Hong, S.C.E. Tsang, Electronic modulation of a copper/zinc oxide catalyst by a heterojunction for selective hydrogenation of carbon dioxide to methanol, Angew. Chem., Int. Ed. 51 (2012) 5832–5836.

[81] H. Jeong, C. Cho, T. Kim, Effect of Zr and pH in the preparation of Cu/ZnO catalysts for the methanol synthesis by CO$_2$ hydrogenation, J React Kinet Mech Catal 106 (2012) 435–443.

[82] H. Ren, C.H. Xu, H.Y. Zhao, Y.X. Wang, J. Liu, Methanol synthesis from CO$_2$

hydrogenation over Cu/γ-Al$_2$O$_3$ catalysts modified by ZnO, ZrO$_2$ and MgO, J Ind Eng Chem 28 (2015) 261–267.

[83] W. Cai, P.R. de la Piscina, J. Toyir, N. Homs, CO$_2$ hydrogenation to methanol over CuZnGa catalysts prepared using microwave-assisted methods, Catal. Today 242 (2015) 193–199.

[84] O. Tursunov, L. Kustov, Z. Tilyabaev, Methanol synthesis from the catalytic hydrogenation of CO$_2$ over CuO-ZnO supported on aluminum and silicon oxides, J Taiwan Inst Chem Eng 78 (2017) 416–422.

[85] X. Dong, F. Li, N. Zhao, F. Xiao, J. Wang, Y. Tan, CO$_2$ hydrogenation to methanol over Cu/ZnO/ZrO2 catalysts prepared by precipitation-reduction method, J Appl Catal B 191 (2016) 8–17.

[86] V.Y. Gusev, X. Feng, Z. Bu, G.L. Haller, J.A. O'Brien, Mechanical stability of pure silica mesoporous MCM-41 by nitrogen adsorption and small-angle X-ray diffraction measurements, J. Phys. Chem. B 100 (1996) 1985–1988.

[87] R. Mokaya, Improving the stability of mesoporous MCM-41 silica via thicker more highly condensed pore walls, J. Phys. Chem. B 103 (1999) 10204–10208.

[88] K. Cassiers, T. Linssen, M. Mathieu, M. Benjelloun, K. Schrijnemakers, P. Van Der Voort, P. Cool, E.F. Vansant, A detailed study of thermal, hydrothermal, and mechanical stabilities of a wide range of surfactant assembled mesoporous silicas, Chem. Mater. 14 (2002) 2317–2324.

[89] M. Kurtz, H. Wilmer, T. Genger, O. Hinrichsen, M. Muhler, Deactivation of supported copper catalysts for methanol synthesis, Catal. Lett. 86 (2003) 77–80.

[90] H. Lei, R. Nie, G. Wu, Z. Hou, Hydrogenation of CO$_2$ to CH$_3$OH over Cu/ZnO catalysts with different ZnO morphology, Fuel 154 (2015) 161–166.